LANGMUIR

pubs.acs.org/Langmuir Article

Deposition Behavior of Polyaniline on Carbon Nanofibers by Oxidative Chemical Vapor Deposition

Xiaobo Li, Ayda Rafie, Vibha Kalra, and Kenneth K. S. Lau*



Cite This: Langmuir 2020, 36, 13079-13086



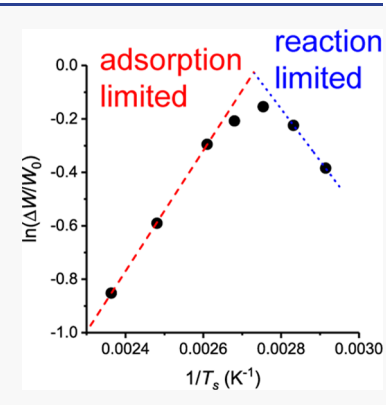
ACCESS

Metrics & More

Article Recommendations

3 Supporting Information

ABSTRACT: Oxidative chemical vapor deposition (oCVD) offers unique advantages as a liquid-free processing technique in synthesizing and integrating conducting polymers, including polyaniline (PANI), by enabling conformal coatings onto nanostructured substrates, like carbon nanofibers. With relatively thick nanofiber mats, the challenge is to ensure uniform coating thickness through the porous substrates. Here, the substrate temperature during oCVD is found to be a primary factor influencing PANI coating uniformity. Coating uniformity is enhanced by operating at a higher substrate temperature, where monomer adsorption is believed to be limiting relative to intrinsic reaction kinetics. Also, a higher substrate temperature leads to significantly less PANI oligomers and more PANI in the emeraldine oxidation state. A systematic study of oCVD kinetics with substrate temperature shows a reaction-limited regime at lower substrate temperatures with an activation energy of 12.0 kJ/mol, which is believed to be controlled by the self-catalyzed PANI polymerization reaction that transitions at higher substrate temperatures above 90 °C to an adsorption-limited regime as indicated by a negative activation energy of −18.8 kJ/mol. Overall, by operating within an



adsorption-limited oCVD regime, more uniform oCVD PANI coatings on electrospun carbon nanofiber mats have been achieved.

■ INTRODUCTION

Polyaniline (PANI) coatings onto substrates with a high surface area have found applications in many fields, including electrocatalysts for oxygen reduction reaction processes, 1-3 gas sensors, 4-6 supercapacitors, 7-9 and lithium sulfur batteries. However, conventional liquid-based coating methods cannot make very conformal, uniform, and thin coatings onto high specific area substrates, which can negatively impact performance in application areas. These methods can result in coating irregularities, aggregation, cracks, and nonconformal coatings because of poor surface wettability and liquid surface tension forces. 13,14 Specific examples of PANI coatings on carbon nanomaterials have directly shown that liquid-based methods often result in nonconformal and nonuniform coatings. 15-17 To overcome these challenges, the oxidative chemical vapor deposition (oCVD) process is introduced as a more effective way to make more conformal and uniform PANI coatings. Instead of utilizing a liquid solvent for coating, oCVD utilizes gas-phase reactants under low pressures to directly synthesize and grow PANI as thin coatings. Briefly, the aniline monomer and a chemical oxidant, such as antimony pentachloride (SbCl₅), are vaporized and continuously delivered into a reactor chamber, where the oxidant enables the oxidative polymerization of aniline to form PANI on a substrate surface. As a general technique, oCVD has been shown previously to produce conformal coatings of conducting polymers, such as polythiophene and poly(3,4ethylenedioxythiophene) (PEDOT) and PANI, on different

carbon materials, including activated carbon, carbon cloth, carbon nanotubes, and carbide-derived carbon. $^{18-21}$

In our previous work with oCVD PANI, conformal PANI coatings have been formed on freestanding carbon nanofiber (CNF) mats made through electrospinning. 22 The conformal PANI coatings yield enhanced and more stable charge storage as electrodes in supercapacitor devices. However, processingwise, we find that it is challenging to produce PANI coatings with a uniform coating thickness throughout the thickness of the CNF mats (typically $\sim 25 \mu m$). Coating is predominantly confined to the surface region of the mats exposed to the reactant vapors. The previous work also relied on a postdeposition washing step with tetrahydrofuran (THF) solvent to remove residual oligomers formed during the PANI polymerization process. These oligomers are undesirable as they degrade coating and device properties. Also, the added washing step complicates the overall process scheme, makes it not fully liquid-free, and creates a greater environmental footprint. Thus, we seek to form PANI coatings on CNFs with the goals of achieving a more uniform coating thickness

Received: August 27, 2020 Revised: October 7, 2020 Published: October 23, 2020





throughout the CNF mat, and implementing a simpler, all-dry, and more environmentally friendly oCVD process scheme.

To this end, we probe the effect of substrate temperature on oCVD PANI coatings on CNFs in order to control polymerization kinetics and polymer structure through oCVD processing. Prior literature work on oCVD of other conducting polymers has found the substrate temperature as a dominant processing parameter in influencing polymer structure and properties. 23,24 For example, in the oCVD of polyisothianaphthene (PITN), the color and transparency of the PITN film can be systematically varied by changing substrate temperature.²⁴ Previous oCVD work on PEDOT has also shown that an increase in substrate temperature can yield more porous films¹⁴ and an increase in electrical conductivity, which is attributed to a greater polymer conjugation length and a loss of oligomer at the higher temperatures.²³ In other polymer chemical vapor deposition (CVD) work, such as initiated CVD (iCVD) of acrylate polymers, substrate temperature is a key parameter controlling monomer adsorption, surface diffusion, and surface polymerization, factors that determine coating uniformity on porous, nanostructured substrates.²⁵ Here, we report a systematic study of the effect of substrate temperature on the oCVD deposition kinetics of PANI with the aim of using substrate temperature to directly control polymer structure and coating uniformity.

EXPERIMENTAL SECTION

CNF Fabrication. Electrospinning was used to prepare CNF mats based on our previously established procedures. ^{26,27} To prepare the solution for electrospinning, polyacrylonitrile (PAN, average $M_{\rm w}$ 150,000, Sigma-Aldrich) and dried LIQION (Nafion, Liquion 1105, Ion Power Inc.) were dissolved in N,N-dimethylformamide (DMF, Sigma-Aldrich) overnight. PAN and Nafion were then mixed in a 40:60 weight ratio with a total solid concentration of 18% in DMF. During electrospinning, the distance between the aluminum foilgrounded collector and the needle tip (22-gauge stainless steel needle, Hamilton Co.) was kept between 5 and 6". Relative humidity inside the spinning setup was kept below 20% and a solution flow rate was set to 0.2 mL/h using a syringe pump (New Era Pump Systems, Inc.). An applied voltage of 9-10 kV was used to obtain a freestanding mat. In order to make porous CNF (pCNF) samples, the electrospun nanofiber mats were first stabilized in a convection oven (Binder Inc.) at 280 °C for 6 h in air. After the stabilization step, the mats were carbonized in a tube furnace (MTI corporation) at 1000 °C for 1 h (with a heating rate of 3 °C/min) under continuous nitrogen flow. The mats were then cut using a 1" (2.54 cm) diameter punch and dried at 140 °C under air. Then, the mats were weighed using a precision microbalance (Mettler Toledo) with a sensitivity of 0.01 mg to determine their initial sample weight. The initial weight of the mats was chosen to be within a desired range of 3.10-3.75 mg that averages to around 3.50 mg. Based on previous nitrogen sorption measurements, the individual fibers possess intrinsic micro and mesoscale porosity that yield a surface area of ~680 m²/g.²

oCVD PANI Synthesis and Coating. PANI was synthesized from vaporized monomer aniline (99.5%, Sigma-Aldrich) and oxidant antimony pentachloride (SbCl₅, 99.99% trace metal basis, Sigma-Aldrich), both used as received, in a custom-built oCVD reactor system. A schematic diagram of the oCVD reactor system is shown in Figure 1a. The aniline monomer was fed through inlet ports on one side of the reactor framework, while the SbCl₅ oxidant was fed separately through a 0.25" diameter feedthrough line directly into the monomer flow. Both reactants were heated to 60 °C in source containers to ensure a sufficient vapor head space in order to deliver a constant flow set at 1.5 sccm using low-flow precision metering valves (Swagelok). Inert N₂ carrier gas was used to aid delivery of each reactant through a set flow of 1.5 sccm that was controlled by mass flow controllers (MKS Instruments, model 1479A). Figure 1b shows a

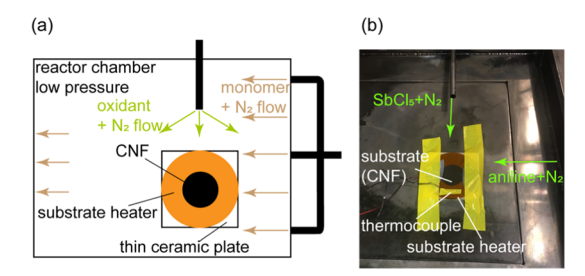


Figure 1. (a) Schematic diagram showing top-down view of the oCVD reactor chamber, and (b) photo showing top-down view of the substrate setup.

photo of the actual setup inside the reactor, showing the reactant flows relative to the substrate placement. The pCNF substrate was placed on a thin film heater (McMaster-Carr), and the substrate temperature was directly controlled using a temperature controller (Omega Engineering) that continuously monitors the substrate temperature through an attached K-type thin wire thermocouple (Omega Engineering). To minimize heat loss from the heater to the reactor stage, a thin ceramic insulator block was placed in between the heater and the stage. Silicon spacers and adhesive tape were used to hold the substrate in position. Additionally, to maintain a more constant reactor environment, the reactor glass lid was heated and kept at 80 °C during the deposition. Depositions were carried out at a reactor pressure of 60 mTorr, maintained using a pressure controller (MKS Instruments) connected to a downstream throttle valve (MKS Instruments) and a capacitance manometer gauge (MKS Instruments) that monitored reactor pressure. Deposition time was set at 1 h for each run. After deposition, the sample was weighed again to determine the weight gain due to PANI growth. Further characterization was made on the sample without any subsequent postdeposition treatment.

Sample Characterization. Fourier-transform infrared (FTIR) spectra were acquired using a Thermo Nicolet 6700 spectrometer in attenuated total reflectance mode with a DTGS detector at 4 cm⁻¹ resolution and averaged over 128 scans. X-ray photoelectron spectroscopy (XPS) analysis was carried out using a Physical Electronics VersaProbe 5000 spectrometer with a microfocused monochromatic scanned X-ray beam equipped with an Al K α X-ray source (1486 eV photons). High-resolution elemental N 1s, Sb 3d5, and Cl 2p spectra were acquired at 50 W using a 200 μ m spot size, 23.500 eV pass energy, and 0.050 eV energy step at 50 ms per step. Scanning electron microscopy (SEM) images were acquired via a Zeiss Supra 50VP with an in-lens detector at 5 kV and a working distance of ~3.4 mm. The images were taken with line integration and seven repeats. Before SEM analysis, the samples were sputtered with Pt/Pb for 40 s to minimize sample charging. From the SEM images, the coated fiber diameters on each side of the sample were measured by ImageJ software with the DiameterJ plugin.²⁹ Measurements were made at six different sample locations and picking four different threshold images generated by the software at each location. These yielded 24 separate measurements from which the average diameter and standard deviation were calculated. For the bare, uncoated fibers, five different sample locations were chosen and four different threshold images were taken from each location, which yielded 20 measurements for deriving the average diameter and standard deviation. See the Supporting Information for more details and the complete set of raw data.

■ RESULTS AND DISCUSSION

oCVD PANI Film Chemistry. To understand the effect of substrate temperature on oCVD PANI film chemistry, substrate temperatures in the range of 70–130 °C were probed, and the corresponding FTIR spectra were acquired, as shown in Figure 2. At lower substrate temperatures of 70 and 90 °C, we see distinct peaks related to PANI oligomers

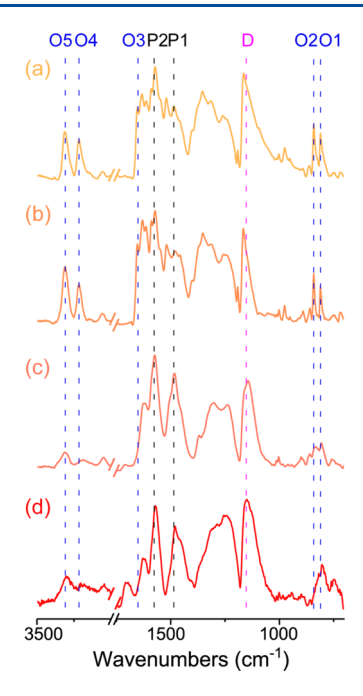


Figure 2. FTIR spectra of oCVD PANI deposited at different substrate temperatures of (a) 70, (b) 90, (c) 110, and (d) 130 °C. The O1 to O4 peaks are associated with short chain oligomers, the P1 and P2 peaks are related to long-chain polymers, and the D peak represents the doping level.

(labeled O1 to O4). The O1 and O2 peaks located at around 800 cm⁻¹ are assigned to CH out-of-plane bending and out-ofplane ring deformation of monosubstituted phenylene rings associated with short-chain oligomers. 30 Likewise, oligomer units are identifiable with the O3 peak at 1630 cm⁻¹ because of NH scissoring vibrations of aromatic amines or the presence of phenazine units,³⁰ and the O4 and O5 peaks at 3220 and 3320 cm⁻¹, which are assigned to hydrogen-bonded NH vibrations and free NH stretching, respectively.³⁰ At higher substrate temperatures of 110 and 130 °C, the peaks related to PANI oligomers become significantly diminished, while the peaks associated with long-chain PANI polymer (labeled P1 and P2) are distinctly stronger. The P1 and P2 peaks at 1460 and 1580 cm⁻¹ represent the benzenoid and quinoid PANI structures, which are the reduced and oxidized PANI forms, respectively. 31 At the highest substrate temperature of 130 °C, the O1 and O2 peaks are replaced by a single peak that can be assigned to the para-coupling of aniline units in the long-chain PANI polymer. 30,32 At all substrate temperatures, there is a peak at 1150 cm⁻¹ (labeled D) that relates to the vibrational mode of $B-N^+H=Q$ or $B-N^+H-B$ structures, which qualitatively describes the extent of doping in PANI.³¹ In oCVD, doping is achieved simultaneously during polymerization because the oxidant acts to oxidize not only the monomer to enable chemical oxidative polymerization but also acts to oxidize and dope the polymer.2

By increasing substrate temperature, the FTIR spectra indicate that the oligomeric content of oCVD PANI can be significantly suppressed. Especially at 130 °C, all the O peaks are barely discernible, which suggests that the deposited film consists mainly of the long-chain PANI polymer. This agrees with previous work on oCVD of other conducting polymers, like PEDOT, which also reported less oligomers and higher polymer conjugation length at higher substrate temperatures.²³ The loss of oligomers can be attributed to a greater chemical

reactivity, in general, at higher reaction temperatures that favor longer-chain growth, and the lower likelihood of oligomers to be thermally stable as a solid at higher surface temperatures. In addition, the FTIR data qualitatively indicate a change in the oxidation level of PANI with varying substrate temperature through the ratio of the relative peak intensities of P2 to P1. This P2-to-P1 ratio provides the proportion of quinoid (oxidized) to benzenoid (reduced) forms of the PANI chemical repeat unit structure, where the ratio of 0:100, 50:50, and 100:0 refers to, respectively, the fully reduced leucoemeraldine, semioxidized emeraldine, and fully oxidized pernigraniline oxidation state of PANI. At lower substrate temperatures of 70 and 90 °C, P2 is much higher in intensity than P1, which indicates that PANI is highly oxidized, approaching that of pernigraniline. At higher substrate temperatures, P2 and P1 peaks are much more similar in intensity, which indicates that PANI is approaching more of the emeraldine state. Thus, by using a higher substrate temperature, oCVD PANI can be formed without the presence of any appreciable amount of oligomers and with a more desirable emeraldine oxidation state, which is well known to have the greatest electrical conductivity among different PANI states.33,34 This overcomes our challenge previously of requiring a postdeposition solvent washing step to remove short-chain oligomers deposited at lower substrate temperature that were found to severely impede PANI performance because of their lower chemical and redox stability.²

To more quantitatively elucidate oCVD PANI film chemistry, higher-resolution N 1s XPS spectra were taken of samples deposited at substrate temperatures in the range of 70–130 °C, as shown in Figure 3. Four distinct nitrogen

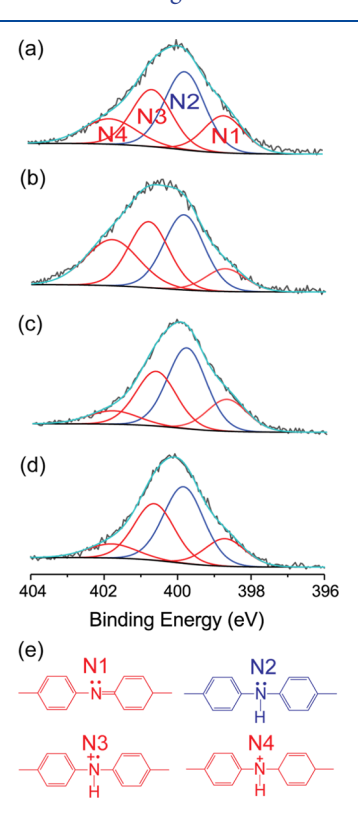


Figure 3. High-resolution N 1s XPS spectra of oCVD PANI deposited at (a) 70, (b) 90, (c) 110, and (d) 130 °C, and their resolved peaks that correspond to (e) different nitrogen bonding environments.

bonding environments can be resolved: N1 (\sim 398.7 eV; FWHM 1.3 eV) for quinoid, N2 (\sim 399.8 eV; FWHM 1.3 eV) for benzenoid, and N3 (\sim 400.6 eV; FWHM 1.3 eV) and N4 (\sim 401.8 eV; FWHM 1.7 eV) for doped quinoid structures. Based on the resolved peak areas, the fraction of quinoid forms in the samples is evaluated from (N1 + N3 + N4)/N_{total}, see Table 1. At lower substrate temperatures of 70 and 90 °C,

Table 1. Elemental Composition and Chemical State of oCVD PANI Deposited at Different Substrate Temperatures

$T_{\rm sub}$ (°C)	Sb (at. %)	Cl (at. %)	% quinoid (Q/B ratio)
70	12.4	3.5	62% (1.6)
90	21.7	3.2	67% (2.0)
110	4.1	5.9	57% (1.3)
130	6.6	3.2	57% (1.3)

PANI contains more quinoid units relative to benzenoid units, which means an overall oxidation state that is more oxidized and closer to the pernigraniline state. At higher substrate temperatures of 110 and 130 °C, the quinoid fraction approaches that of 50%, or nearly an equal amount of quinoid and benzenoid units, which represents more closely to the semioxidized emeraldine state that is the most electrically conductive PANI state. These observations are consistent with the qualitative FTIR analysis above. Based on XPS analysis, Table 1 further shows the amount of antimony (Sb) and chlorine (Cl) present in the oCVD PANI films. These elements are because of the SbCl₅ oxidant and represent the dopant present in these films. The highest amount of dopant, particularly in the amount of Sb, is seen at a substrate temperature of 90 °C, while at much higher substrate temperatures of 110 and 130 °C, the dopant level significantly drops. This trend is mirrored in the resolved N4 peak intensity in Figure 3, which represents the most oxidized nitrogen form. This peak has the highest intensity for the sample at 90 °C, while that for the samples at 110 and 130 °C is significantly reduced. These observations suggest that a maximum oxidized content and maximum doping level are simultaneously achieved at 90 °C, which is also clearly reflected in the highest quinoid fraction at this temperature. This points to the important role of the SbCl₅ oxidant in forming, oxidizing, and doping PANI that seems to be the greatest at 90 °C. From the literature, the generally accepted role of the oxidant is to oxidize the aniline monomer to generate cation radical species, which link together in a step-wise growth to form the PANI

polymer chain.³⁷ In addition, the oxidant also acts as a dopant in oxidizing the formed PANI polymer chain. Because these reactions necessarily occur at the substrate surface, it is understandable why substrate temperature might have a significant impact on the resulting PANI film composition and doping level. As will be discussed further in our kinetics studies below, the change in the level of oxidant seen in PANI with substrate temperature is related to the specific rate process controlling the overall polymer growth.

oCVD PANI Film Morphology. One of the major advantages of oCVD is its ability to coat conformal conducting polymer thin films even within nanoscale structures. This advantage comes from utilizing gas-phase reactants that circumvent the use of liquid solvents in conventional coating methods, which often leads to aggregation, cracks, bridging, blocking, and other film defects because of poor wettability, strong surface tension forces, and capillary effects. By using oCVD, conformal PANI films that wrap around each individual CNF is confirmed in SEM images given in Figure 4. The conformal coatings are also sufficiently thin so that the intrinsic fiber network structure and voids are preserved. The bare, uncoated CNFs show an average diameter of around 200 nm throughout the thickness of the mat and have a slightly rough morphology as seen in the inset images. After oCVD, the PANI-coated CNFs show wider fibers and generally a smoother surface throughout the mat thickness that indicates PANI conformally coated around each individual fiber. It should be noted that the SEM images show top-down views of the fibers on the top (top row) and bottom sides (bottom row) of the CNF mats, where the top side was directly exposed to the gaseous CVD environment while the bottom side was in contact with the substrate heater during oCVD. Thus, the topside fibers have direct access to the gaseous reactants while the bottom-side fibers are expected to be exposed to only those reactants that diffuse through the thickness of the fiber mat. The conformal coatings through the \sim 25 μ m thick mat indicate efficient reactant diffusion that provided sufficient monomer and oxidant for polymerization down to the bottom of the CNF mats.

More closer inspection, however, shows that the bottom sides are relatively thinner compared to the top sides of the mat, which suggests that the top side closest to the gaseous environment still had slightly greater exposure to reactant species that lead to more deposition on the top side compared to the bottom side. Also, the bottom side is expected to be

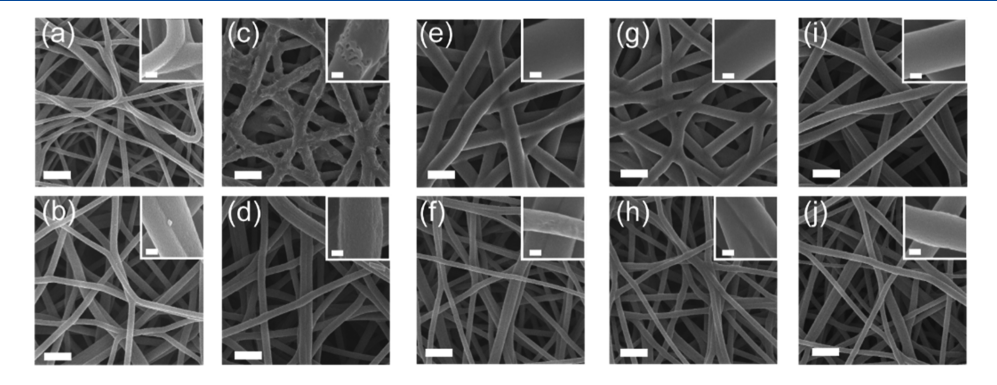


Figure 4. SEM images of bare CNFs (a,b), and oCVD PANI-coated CNFs deposited at (c,d) 70, (e,f) 90, (g,h) 110, and (i,j) 130 °C, showing top-down views of the top (top row) and bottom (bottom row) sides of the CNF mat. During oCVD, the top side was directly exposed to the reactant gas flow while the bottom side was in contact with the substrate heater. Scale bar is 1 μ m (inset is 100 nm).

slightly hotter because of the closer contact with the substrate heater, which discourages precursor adsorption and reduces the sticking coefficient of reactant species on the fiber surface that could further limit surface polymerization. Additionally, diffusion resistance of the reactants through the CNF mat might limit access to reactants at the bottom, which could further slow down the deposition process. More careful inspection also reveals that the coating morphology at 70 °C is somewhat different compared to the other substrate temperatures, with a rougher texture particularly on the top surface. Because this is not observed at the other substrate temperatures, this could indicate a secondary deposition process facilitated by the lower temperature, and might potentially be related to the appreciable oligomers, as indicated by FTIR, that nucleate and form more easily at the exposed top surface. Literature work have shown, both experimentally and through theory and simulations, that short-chain oligomers tend to segregate and bloom at the surface as they are enthalpically and entropically more favored to be at the surface compared to long polymer chains.³⁸ This would lead to surfaces that are not homogeneous with surface irregularities that could explain what is observed in Figure 4c. It is, therefore, likely that the nonhomogeneities at the top CNF mat surface, together with the FTIR support, point to significant oligomer formation at the lowest substrate temperature of 70 °C that was studied.

oCVD PANI Deposition Kinetics. In an attempt to understand more clearly the effect of substrate temperature on deposition behavior, the oCVD PANI growth kinetics were examined. The growth was probed by two independent measuring techniques. First, growth is expressed as an increase in the fiber diameter after deposition. Second, growth is characterized by an increase in sample weight after deposition. It should be noted that because each deposition was run for 1 h, the average deposition rate is equivalent to the total amount of film deposited, either represented by the fiber diameter or weight gain. While weight changes were directly calculated from weight measurements before and after deposition using a weighing balance, the fiber diameters were measured from SEM images using ImageJ with the DiameterJ plugin.²⁹ The fiber diameter for each sample is based on averaging a total of 24 measurements for coated fibers and 20 measurements for uncoated fibers from SEM images. Both the fiber diameter and the weight gain data of oCVD PANI-coated CNFs deposited at different substrate temperatures are shown in Figure 5. The fiber diameter results in Figure 5a include not only the average diameters of fibers coated at different substrate temperatures, but also the spread or difference in the diameters between the top and bottom of the fiber mats, which gives a quantitative measure of the relative coating uniformity through the fiber mat layer. The diameter data clearly show a maximum average diameter of 389 nm for fibers coated at a substrate temperature of 90 °C, which is an increase of 178 nm over the bare fiber diameter of 211 nm (shown as the dashed line to denote the baseline value). Corresponding to this maximum fiber diameter is the maximum diameter spread at 90 °C, that is, the thickest PANI coating also yields the most nonuniform coating or largest spread, with the thickness at the top being 165 nm thicker than at the bottom of the mat. As substrate temperature increases beyond 90 °C, although the coated fiber diameter gradually decreases, the spread also correspondingly decreases to the point where at 150 °C, the spread drops to 22

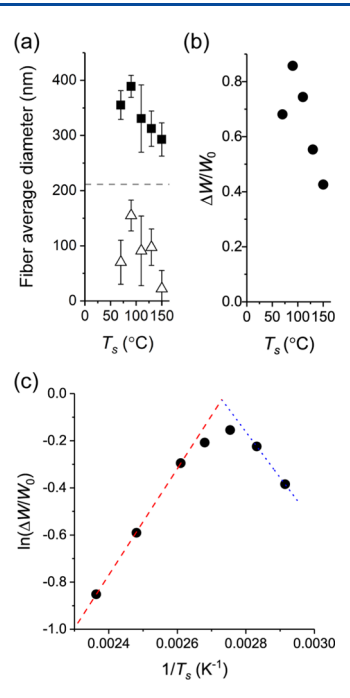


Figure 5. (a) Average fiber diameter (\blacksquare) and diameter spread between the top and bottom fibers (\triangle) of oCVD PANI-coated CNFs deposited at different substrate temperatures (dashed line is the average or baseline diameter of uncoated CNFs). (b) Sample weight gain (ΔW) over the bare fiber weight (W_0) of oCVD PANI-coated CNFs deposited at different substrate temperatures, and (c) the associated Arrhenius plot. Note that each deposition run was 1 h so the coating amount in terms of diameter or weight is equivalent to an average deposition rate.

nm while maintaining a respectable coated fiber diameter of 293 nm or a PANI coating thickness of 82 nm.

The weight gain data, plotted in Figure 5b, shows the weight gain or the weight of PANI for samples deposited at various substrate temperatures normalized to the initial weight of the uncoated bare fibers. Again, a maximum weight gain or the largest amount of PANI is seen at a substrate temperature of 90 °C, and similar to the fiber diameter results, the deposition amount is lower or equivalently the deposition rate (since each run is for the same time of 1 h) slows down on either side of 90 $^{\circ}\text{C}$ for the temperatures studied. We used this relative weight gain data and plotted this as an Arrhenius relation to derive activation energies, as shown in Figure 5c. Note that this plot contains additional weight gain data at substrate temperatures of 80 and 100 °C to more clearly capture the maximum at 90 °C. Clearly, there are two distinct temperature relations that can be seen and which can be fitted to two linear relations, one on each side to this maximum. To the right side, or at lower substrate temperatures, a linear fit yields an activation energy of 12.0 kJ/mol, while to the left side, or at higher substrate temperatures, the linear fit yields a negative activation energy of -18.8 kJ/mol. The positive activation energy of 12.0 kJ/mol is lower than that reported by some for the oxidative polymerization of aniline in solution, which is in the range of 40-44 kJ/mol.³⁹⁻⁴¹ However, these kinetic studies did not relate their values to any specific rate equation or reaction mechanism. In the oxidative polymerization of aniline, the most commonly accepted reaction mechanism involves a direct one-electron transfer from the aniline monomer to the oxidant (i.e., aniline oxidation) to form cation radical species, which then induce step-wise polymer

chain growth.⁴² However, studies have found that there is a second reaction pathway that is autocatalyzed by the presence of the PANI polymer, which significantly accelerates aniline oxidation and polymerization.^{43–47} It is believed that the oxidized pernigraniline PANI state is able to promote aniline oxidation to cation radicals, but its exact role remains a subject of debate.³⁷ Kinetic studies considering these two reaction pathways in parallel have found that the rate coefficient of the PANI-catalyzed reaction is several orders of magnitude larger than without the aid of PANI when the reaction rate is modeled by the following rate equation (where M is the aniline monomer and Ox is the oxidant)^{44,48}

rate =
$$-\frac{d[M]}{dt}$$
 = $k_1[M][Ox] + k_2[M][PANI]$

Furthermore, kinetic studies of aniline polymerization that decouple the activation energies of the two contributions have found the first one to be in the range of 29-81 kJ/mol while the second PANI-catalyzed one is much lower at 17-19 kJ/mol. 37,49 In another report for the case of 2-methoxyaniline polymerization, which is believed to follow a similar parallel reaction pathway mechanism, the two activation energies are reported as 57 and 10 kJ/mol, respectively. 50 Given that our value of 12.0 kJ/mol derived from Figure 5c is closer to the activation energy values for the second reaction pathway (k_2), this seems to suggest that the oCVD reaction dependence on substrate temperature below 90 °C is most likely dominated by the PANI-autocatalyzed reaction. Therefore, the above general rate equation simplifies to

rate(low
$$T_{\text{sub}}$$
) = $-\frac{\text{d[M]}}{\text{d}t} \approx k_2[\text{M}][\text{PANI}]$

Because oCVD naturally confines the polymerization process to be at the surface where PANI is being deposited, it is reasonable to believe that PANI would have a dominating impact on the observed oCVD reaction kinetics. Furthermore, the literature has suggested that the autocatalytic mechanism could be because of a rapid electron transfer specifically from cation radicals of PANI oligomers to the monomer. Escause our FTIR and SEM results support a large amount of oligomer below 90 °C, and our FTIR and XPS results both evidence a more oxidized pernigraniline-like state below 90 °C, it seems reasonable to conclude that the autocatalysis is aided by highly oxidized, short-chain oligomers in this temperature range that leads to the observed oCVD kinetic behavior.

The negative activation energy of -18.8 kJ/mol seen for kinetics at higher substrate temperatures above 90 °C indicates that the polymerization process is no longer reaction-limited but most likely limited by reactant adsorption on the substrate surface because higher temperatures generally reduce vapor-tosurface adsorption (or sticking coefficient) and, therefore, reduce the amount of reactant at a surface available for reaction. It is possible that this negative activation energy (absolute value) is related to the heat of adsorption of aniline monomer vapor on the substrate surface. 52 However, our value is lower than the heat of adsorption values of aniline vapor reported in the literature, for example, 42-50 kJ/mol based on adsorption experiments on graphitized carbon black materials, 53,54 and 66-69 kJ/mol based on Monte Carlo simulations and quantum chemical calculations on an ice surface.⁵⁵ The disparity could be rationalized by recognizing that our value is most likely not simply because of the heat of adsorption but an effective activation energy that accounts for both adsorption

and surface reaction. At high substrate temperatures, it is possible that the autocatalytic contribution becomes small, given the lack of oligomer content and less-oxidized PANI from our spectroscopic studies. Thus, the rate could be dominated by the first reaction pathway (k_1) and so the general rate equation simplifies to

rate(high
$$T_{\text{sub}}$$
) = $-\frac{\text{d}[M]}{\text{d}t} \approx k_1[M]_{\text{ad}}[Ox]$
= $k_1 K_M[M][S][Ox]$

where we recognize that the monomer in the oCVD process must necessarily adsorb before the reaction occurs, and so its concentration can be related to the monomer adsorption constant $K_{\rm M}$ (where S refers to the surface site for monomer adsorption). Based on this rate equation, the effective rate coefficient is $k_{\rm eff} = k_1 K_{\rm M}$, and so the effective activation energy is $E_{\rm eff} = E_1 - \Delta H_{\rm ad}$ because $k_1 \sim {\rm e}^{-E_1/(RT)}$ and $K_{\rm M} \sim {\rm e}^{\Delta H_{\rm ad}/(RT)}$. Thus, we can now rationalize our experimental value of -18.8kJ/mol as a net activation energy where $\Delta H_{\rm ad} > E_1$ ($E_{\rm eff} < 0).$ As discussed above, reported values of ΔH_{ad} are quite high, in the range of 42-69 kJ/mol, while the reported values of E_1 have a broad range of 29-81 kJ/mol that depends on the reaction environment and oxidant used. Therefore, it is possible by using the lower end values of $\Delta H_{\rm ad}$ and E_1 that a negative effective activation energy in the ballpark of our experimental value can be attained. Regardless, the net activation energy supports an adsorption-limited process that slows down deposition kinetics, thereby favoring more efficient reactant diffusion through the CNF mat, which leads to more uniform PANI deposition across the mat thickness.

CONCLUSIONS

In this work, substrate temperature is found to be a key oCVD process parameter impacting the chemical and physical nature of deposited PANI films. A significant oligomer fraction and more oxidized PANI are found at lower deposition temperatures, while at higher temperatures above 90 °C, long-chain PANI closer to the emeraldine state is obtained. This helps to simplify processing because previously a postdeposition washing step was required to remove oligomers where oCVD PANI was deposited at lower substrate temperatures. PANI coatings on CNFs are found to be very conformal that preserve the intrinsic fiber mat architecture without any issues associated with liquid processing, which tend to lead to aggregation, cracks, bridging, and blockages. Coating uniformity through the mat layer thickness was found to be better at higher substrate temperatures where PANI growth is slower, which facilitates reactant mass transport. A kinetic analysis that looked at both the fiber diameter increase and PANI weight gain found a maximum rate at 90 °C that divided the deposition behavior into two distinct regions. At substrate temperatures lower than 90 °C, a reaction-limited behavior is observed with an activated energy of 12.0 kJ/mol that could be related to the autocatalytic polymerization that is mediated by the presence of oxidized PANI. At substrate temperatures higher than 90 °C, a negative activation energy of −18.8 kJ/ mol indicated a reaction environment that is controlled by monomer adsorption, which determines the amount of surface monomer available for polymerization.

ASSOCIATED CONTENT

Supporting Information

The Supporting Information is available free of charge at https://pubs.acs.org/doi/10.1021/acs.langmuir.0c02539.

Fiber diameter measurement; SEM images of bare carbon nanofibers and the corresponding black and white threshold images automatically generated using DiameterJ; and raw fiber diameter measurements made through ImageJ analysis using the DiameterJ plugin (PDF)

AUTHOR INFORMATION

Corresponding Author

Kenneth K. S. Lau — Department of Chemical and Biological Engineering, Drexel University, Philadelphia, Pennsylvania 19104, United States; orcid.org/0000-0002-7733-1233; Email: @drexel.edu

Authors

Xiaobo Li — Department of Chemical and Biological Engineering, Drexel University, Philadelphia, Pennsylvania 19104, United States

Ayda Rafie — Department of Chemical and Biological Engineering, Drexel University, Philadelphia, Pennsylvania 19104, United States

Vibha Kalra — Department of Chemical and Biological Engineering, Drexel University, Philadelphia, Pennsylvania 19104, United States; ⊙ orcid.org/0000-0002-2630-1560

Complete contact information is available at: https://pubs.acs.org/10.1021/acs.langmuir.0c02539

Author Contributions

X.L. conducted all the oCVD experiments and related materials characterization, and wrote most of the manuscript. A.R. prepared the CNF substrates and wrote the experimental procedure for nanofiber fabrication. V.K. provided oversight to the nanofiber synthesis. K.K.S.L. managed the rest of the work in the manuscript. All authors reviewed and gave approval to the final version of the manuscript.

Notes

The authors declare no competing financial interest.

ACKNOWLEDGMENTS

The authors would like to thank the U.S. National Science Foundation for funding support through award no. CMMI-1463170. In addition, X.L. and K.K.S.L. would like to acknowledge further NSF support through award no. CMMI-1950964. The authors would like to also acknowledge the use of Drexel University's Centralized Research Facilities.

REFERENCES

- (1) Wu, G.; More, K. L.; Johnston, C. M.; Zelenay, P. High-Performance Electrocatalysts for Oxygen Reduction Derived from Polyaniline, Iron, and Cobalt. *Science* **2011**, 332, 443–447.
- (2) Zhang, J.; Zhao, Z.; Xia, Z.; Dai, L. A metal-free bifunctional electrocatalyst for oxygen reduction and oxygen evolution reactions. *Nat. Nanotechnol.* **2015**, *10*, 444–452.
- (3) Liang, H.-W.; Wei, W.; Wu, Z.-S.; Feng, X.; Müllen, K. Mesoporous Metal-Nitrogen-Doped Carbon Electrocatalysts for Highly Efficient Oxygen Reduction Reaction. *J. Am. Chem. Soc.* **2013**, *135*, 16002–16005.
- (4) Huang, X.; Hu, N.; Gao, R.; Yu, Y.; Wang, Y.; Yang, Z.; Siu-Wai Kong, E.; Wei, H.; Zhang, Y. Reduced graphene oxide-polyaniline

- hybrid: Preparation, characterization and its applications for ammonia gas sensing. *J. Mater. Chem.* **2012**, *22*, 22488–22495.
- (5) Wu, Z.; Chen, X.; Zhu, S.; Zhou, Z.; Yao, Y.; Quan, W.; Liu, B. Enhanced sensitivity of ammonia sensor using graphene/polyaniline nanocomposite. *Sens. Actuators B-Chem.* **2013**, *178*, 485–493.
- (6) Song, E.; Choi, J.-W. Conducting Polyaniline Nanowire and Its Applications in Chemiresistive Sensing. *Nanomaterials* **2013**, *3*, 498–523
- (7) Zhou, K.; He, Y.; Xu, Q.; Zhang, Q. E.; Zhou, A. A.; Lu, Z.; Yang, L.-K.; Jiang, Y.; Ge, D.; Liu, X. Y.; Bai, H. A Hydrogel of Ultrathin Pure Polyaniline Nanofibers: Oxidant-Templating Preparation and Supercapacitor Application. *ACS Nano* **2018**, *12*, 5888–5894.
- (8) Ren, X.; Fan, H.; Ma, J.; Wang, C.; Zhang, M.; Zhao, N. Hierarchical Co3O4/PANI hollow nanocages: Synthesis and application for electrode materials of supercapacitors. *Appl. Surf. Sci.* **2018**, *441*, 194–203.
- (9) Li, P.; Jin, Z. Y.; Peng, L. L.; Zhao, F.; Xiao, D.; Jin, Y.; Yu, G. H. Stretchable All-Gel-State Fiber-Shaped Supercapacitors Enabled by Macromolecularly Interconnected 3D Graphene/Nanostructured Conductive Polymer Hydrogels. *Adv. Mater.* **2018**, *30*, 1800124.
- (10) Xiao, L.; Cao, Y.; Xiao, J.; Schwenzer, B.; Engelhard, M. H.; Saraf, L. V.; Nie, Z.; Exarhos, G. J.; Liu, J. A Soft Approach to Encapsulate Sulfur: Polyaniline Nanotubes for Lithium-Sulfur Batteries with Long Cycle Life. *Adv. Mater.* **2012**, *24*, 1176–1181.
- (11) Li, W.; Zhang, Q.; Zheng, G.; Seh, Z. W.; Yao, H.; Cui, Y. Understanding the Role of Different Conductive Polymers in Improving the Nanostructured Sulfur Cathode Performance. *Nano Lett.* **2013**, *13*, 5534–5540.
- (12) Hu, H.; Cheng, H.; Liu, Z.; Li, G.; Zhu, Q.; Yu, Y. In Situ Polymerized PAN-Assisted S/C Nanosphere with Enhanced High-Power Performance as Cathode for Lithium/Sulfur Batteries. *Nano Lett.* **2015**, *15*, 5116–5123.
- (13) Alf, M. E.; Asatekin, A.; Barr, M. C.; Baxamusa, S. H.; Chelawat, H. Chemical vapor deposition of conformal, functional, and responsive polymer films. *Adv. Mater.* **2010**, *22*, 1993–2027.
- (14) Im, S. G.; Kusters, D.; Choi, W.; Baxamusa, S. H.; van de Sanden, M. C. M.; Gleason, K. K. Conformal coverage of poly(3,4-ethylenedioxythiophene) films with tunable nanoporosity via oxidative chemical vapor deposition. *ACS Nano* **2008**, *2*, 1959–1967.
- (15) Shen, K.-w.; Ran, F.; Tan, Y.-t.; Niu, X.-q.; Fan, H.-l.; Yan, K.; Kong, L.-b.; Kang, L. Toward interconnected hierarchical porous structure via chemical depositing organic nano-polyaniline on inorganic carbon scaffold for supercapacitor. *Synth. Met.* **2015**, *199*, 205–213.
- (16) Kaitsuka, Y.; Hayashi, N.; Shimokawa, T.; Togawa, E.; Goto, H. Synthesis of Polyaniline (PANI) in Nano-Reaction Field of Cellulose Nanofiber (CNF), and Carbonization. *Polymers* **2016**, *8*, 40.
- (17) Wu, K.; Yu, J.; Jiang, X. Multi-walled carbon nanotubes modified by polyaniline for the removal of alizarin yellow R from aqueous solutions. *Adsorpt. Sci. Technol.* **2018**, *36*, 198–214.
- (18) Nejati, S.; Minford, T. E.; Smolin, Y. Y.; Lau, K. K. S. Enhanced charge storage of ultrathin polythiophene films within porous nanostructures. *ACS Nano* **2014**, *8*, 5413–5422.
- (19) Kaviani, S.; Mohammadi Ghaleni, M.; Tavakoli, E.; Nejati, S. Electroactive and Conformal Coatings of Oxidative Chemical Vapor Deposition Polymers for Oxygen Electroreduction. *ACS Appl. Polym. Mater.* **2019**, *1*, 552–560.
- (20) Wang, X.; Ugur, A.; Goktas, H.; Chen, N.; Wang, M.; Lachman, N.; Kalfon-Cohen, E.; Fang, W.; Wardle, B. L.; Gleason, K. K. Room Temperature Resistive Volatile Organic Compound Sensing Materials Based on a Hybrid Structure of Vertically Aligned Carbon Nanotubes and Conformal oCVD/iCVD Polymer Coatings. ACS Sens. 2016, 1, 374–383.
- (21) Smolin, Y. Y.; Van Aken, K. L.; Boota, M.; Soroush, M.; Gogotsi, Y.; Lau, K. K. S. Engineering ultrathin polyaniline in micro/mesoporous carbon supercapacitor electrodes using oxidative chemical vapor deposition. *Adv. Mater. Interfaces* **2017**, *4*, 1601201.

- (22) Li, X.; Rafie, A.; Smolin, Y. Y.; Simotwo, S.; Kalra, V.; Lau, K. K. S. Engineering conformal nanoporous polyaniline via oxidative chemical vapor deposition and its potential application in supercapacitors. *Chem. Eng. Sci.* **2019**, *194*, 156–164.
- (23) Im, S. G.; Gleason, K. K. Systematic control of the electrical conductivity of poly(3,4-ethylenedioxythiophene) via oxidative chemical vapor deposition. *Macromolecules* **2007**, 40, 6552–6556.
- (24) Borrelli, D. C.; Gleason, K. K. Tunable Low Bandgap Polyisothianaphthene via Oxidative Chemical Vapor Deposition. *Macromolecules* **2013**, *46*, 6169–6176.
- (25) Nejati, S.; Lau, K. K. S. Pore Filling of Nanostructured Electrodes in Dye Sensitized Solar Cells by Initiated Chemical Vapor Deposition. *Nano Lett.* **2011**, *11*, 419–423.
- (26) Tran, C.; Kalra, V. Fabrication of porous carbon nanofibers with adjustable pore sizes as electrodes for supercapacitors. *J. Power Sources* **2013**, 235, 289–296.
- (27) Singh, A.; Rafie, A.; Kalra, V. Revisiting the use of electrolyte additives in Li-S batteries: the role of porosity of sulfur host materials. *Sustain. Energy Fuels* **2019**, *3*, 2788–2797.
- (28) Smolin, Y. Y.; Soroush, M.; Lau, K. K. S. Oxidative chemical vapor deposition of polyaniline thin films. *Beilstein J. Nanotechnol.* **2017**, *8*, 1266–1276.
- (29) Hotaling, N. A.; Bharti, K.; Kriel, H.; Simon, C. G. DiameterJ: A validated open source nanofiber diameter measurement tool. *Biomaterials* **2015**, *61*, 327–338.
- (30) Stejskal, J.; Trchová, M. Aniline oligomers versus polyaniline. *Polym. Int.* **2012**, *61*, 240–251.
- (31) Tang, J.; Jing, X.; Wang, B.; Wang, F. Infrared spectra of soluble polyaniline. *Synth. Met.* **1988**, *24*, 231–238.
- (32) Trchová, M.; Šeděnková, I.; Tobolková, E.; Stejskal, J. FTIR spectroscopic and conductivity study of the thermal degradation of polyaniline films. *Polym. Degrad. Stab.* **2004**, *86*, 179–185.
- (33) Macdiarmid, A. G.; Chiang, J.-C.; Halpern, M.; Huang, W.-S.; Mu, S.-L.; Nanaxakkara, L. D.; Wu, S. W.; Yaniger, S. I. "Polyaniline": Interconversion of Metallic and Insulating Forms. *Mol. Cryst. Liq. Cryst.* 1985, 121, 173–180.
- (34) Macdiarmid, A. G.; Chiang, J.-C.; Huang, W.; Humphrey, B. D.; Somasiri, N. L. D. Polyaniline: Protonic Acid Doping to the Metallic Regime. *Mol. Cryst. Liq. Cryst.* **1985**, *125*, 309–318.
- (35) Kumar, S. N.; Bouyssoux, G.; Gaillard, F. Electronic and structural characterization of electrochemically synthesized conducting polyaniline from XPS studies. *Surf. Interface Anal.* **1990**, *15*, 531–536.
- (36) Kumar, S. N.; Gaillard, F.; Bouyssoux, G.; Sartre, A. Highresolution XPS studies of electrochemically synthesized conducting polyaniline films. *Synth. Met.* **1990**, *36*, 111–127.
- (37) Mezhuev, Y. O.; Korshak, Y. V.; Shtil'man, M. I. A new concept of the kinetics and mechanism of the oxidative polymerization of aromatic amines. *Russ. J. Phys. Chem. B* **2015**, *9*, 306–315.
- (38) Sabattié, E. F. D.; Tasche, J.; Wilson, M. R.; Skoda, M. W. A.; Hughes, A.; Lindner, T.; Thompson, R. L. Predicting oligomer/polymer compatibility and the impact on nanoscale segregation in thin films. *Soft Matter* **2017**, *13*, 3580–3591.
- (39) Riede, A.; Helmstedt, M.; Riede, V.; Stejskal, J. Polyaniline dispersions 7. Dynamic light scattering study of particle formation. *Colloid Polym. Sci.* **1997**, 275, 814–820.
- (40) Ayad, M. M.; Gemaey, A. H.; Salahuddin, N.; Shenashin, M. A. The kinetics and spectral studies of the in situ polyaniline film formation. *J. Colloid Interf. Sci.* **2003**, 263, 196–201.
- (41) Jozefowicz, M.; Yu, L. T.; Belorgey, G.; Buvet, R. Conductivité Electronique et Propriétés Chimiques de Polyanilines Oligomères. *J. Polym. Sci. Part C: Polym. Symp.* **1967**, *16*, 2943–2954.
- (42) Sapurina, I.; Stejskal, J. The mechanism of the oxidative polymerization of aniline and the formation of supramolecular polyaniline structures. *Polym. Int.* **2008**, *57*, 1295–1325.
- (43) Wei, Y.; Sun, Y.; Tang, X. Autoacceleration and kinetics of electrochemical polymerization of aniline. *J. Phys. Chem.* **1989**, *93*, 4878–4881.

- (44) Tzou, K.; Gregory, R. V. Kinetic study of the chemical polymerization of aniline in aqueous solutions. *Synth. Met.* **1992**, 47, 267–277.
- (45) Sasaki, K.; Kaya, M.; Yano, J.; Kitani, A.; Kunai, A. Growth mechanism in the electropolymerization of aniline and p-amino-diphenylamine. *J. Electroanal. Chem. Interfacial Electrochem.* **1986**, 215, 401–407.
- (46) Thyssen, A.; Borgerding, A.; Schultze, J. W. Formation and electronic conductivity of polyaniline. *Makromol. Chem. Macromol. Symp.* **1987**, 8, 143–157.
- (47) König, U.; Schultze, J. W. Kinetics of polyaniline formation and redox processes. J. Electroanal. Chem. Interfacial Electrochem. 1988, 242, 243–254.
- (48) Gill, M. T.; Chapman, S. E.; DeArmitt, C. L.; Baines, F. L.; Dadswell, C. M.; Stamper, J. G.; Lawless, G. A.; Billingham, N. C.; Armes, S. P. A study of the kinetics of polymerization of aniline using proton NMR spectroscopy. *Synth. Met.* **1998**, *93*, 227–233.
- (49) Chakraborty, M.; Mukherjee, D. C.; Mandal, B. M. Dispersion Polymerization of Aniline in Different Media: A UV–Visible Spectroscopic and Kinetic Study. *Langmuir* **2000**, *16*, 2482–2488.
- (50) Mav, I.; Zigon, M. 1H NMR study of the kinetics of substituted aniline polymerization. I. Homopolymerization of 2-methoxyaniline. *J. Polym. Sci. Part A: Polym. Chem.* **2001**, *39*, 2471–2481.
- (51) Santhosh, P.; Gopalan, A. I.; Sankarasubramanian, M.; Mathanmohan, T.; Vasudevan, T.; Lee, K.-P. Microstructure and thermal behavior of poly(o-anisidine)/poly(ethylene terephthalate) composite. *Polym. J.* **2005**, *37*, 489–497.
- (52) Lau, K. K. S.; Gleason, K. K. Initiated Chemical Vapor Deposition (iCVD) of Poly(alkyl acrylates): An Experimental Study. *Macromolecules* **2006**, *39*, 3688–3694.
- (53) Kiselev, A. V.; Polotnyuk, E. B.; Shcherbakova, K. D. Gas chromatographic study of adsorption of nitrogen-containing organic compounds on graphitized thermal carbon black. *Chromatographia* 1981, 14, 478–483.
- (54) Yashkina, E. A.; Svetlov, D. A.; Yashkin, S. N. Adsorption of nitrobenzene, aniline and nitroanilines on the surface of a basal face of graphite. *Russ. J. Phys. Chem. A* **2012**, *86*, 1702–1709.
- (55) Fu, Z.; He, N.; Zhou, P. T.; Xie, H. B.; Fu, Z. Q.; Liu, C.; Chen, J. W. Grand canonical Monte Carlo simulation on adsorption of aniline on the ice surface. *J. Mol. Liq.* **2019**, 290, 111221.